December, 2012

# Eddy Current Probe Signals Due to a Crack at a Right-Angled Corner

John R. Bowler, *Iowa State University*
Theodoros P. Theodoulidis
Nicolaos Poulakis

# Eddy Current Probe Signals Due to a Crack at a Right-Angled Corner

John R. Bowler[1], Theodoros P. Theodoulidis[2], and Nikolaos Poulakis[3]

[1]Center for Nondestructive Evaluation, Iowa State University, Ames, Iowa, USA
[2]Department of Mechanical Engineering, University of Western Macedonia, 50100 Kozani, Greece
[3]Department of Electrical Engineering, Technological Educational Institute of Western Macedonia, Koila, 50100, Greece

**In eddy current testing, a flaw in a metal is detected when it gives rise to a change in the electrical impedance of the probe that induces current in the material. Theoretical models and computer codes have been developed to predict the probe signals as an aid to improving inspections and the interpretation of measurements. Model calculations can be efficient for a restricted class of problems in which the conductor geometry is simple, such as an infinite plate or tube. The computational cost is usually low in such cases because dedicated Green's kernels are available, allowing numerical approximations of integral equations to be found using only a few unknowns to represent the field in the flaw region. In this study, the aim has been to perform eddy current calculations on corner cracks efficiently using an approximate Green's function for a conductive quarter-space, thereby extending the class of problems that benefit from the use of a dedicated kernel. The properties of the kernel mean that numerical solutions based on boundary or volume elements can be found for an edge crack by rendering as a discrete approximation only the field at the surface of the flaw or the field within it respectively. Volume element calculations have been carried out to determine the field at a corner crack and from it the probe response. Comparisons of the calculated probe impedance due to edge notches show good agreement with experimental measurements.**

***Index Terms*—Boundary elements, conductive wedge, cracks, eddy current, Green's function, integral equation, nondestructive evaluation, volume elements.**

## I. Introduction

THIS paper examines the problem of computing the quasi-static electromagnetic field due to a corner crack in a conductor excited by an eddy current probe. A well-established scheme for finding the field of a flaw is one based on an electric field integral equation used to get numerically predictions via the moment method [1]–[4]. Provided an integral kernel is available that satisfies the appropriate interface condition for the homogeneous conductor, a solution can be sought by representing only the field at the flaw region in a discrete form. Using a kernel for the particular conductor geometry has the advantage of greatly limiting the number of unknowns required to determine the flaw field but kernels that embody the continuity conditions at material interface are currently available in close form for only a few simple shapes such as a half-space [1], [2], [5], infinite cylinder [6], [7] or a sphere [8], each of which can, if needed, contain piecewise uniform layers. Clearly, it is of great value to extend the number of host conductor shapes for which Green's functions are available in a convenient form for numerical evaluation. The creation of new dedicated kernels is of particular practical benefit if they are constructed for computing the response of cracks near edges since cracks tend to nucleate in such regions. With this aim in view, we have derived an approximate dyadic kernel for the quasi-static field in a conductive quarter-space adjoining a three-quarter space of zero conductivity. The dedicated wedge kernel has been used to compute the eddy current probe signals due to cracks in the region of the edge.

Manuscript received March 11, 2012; revised May 02, 2012; accepted May 23, 2012. Date of publication June 08, 2012; date of current version November 20, 2012. Corresponding author: T. P. Theodoulidis (e-mail: theodoul@uowm.gr).

Color versions of one or more of the figures in this paper are available online at http://ieeexplore.ieee.org.

Digital Object Identifier 10.1109/TMAG.2012.2203918

We apply the domain truncation approach used previously to compute the field of a coil in the presence of a homogeneous right-angled wedge [9], [10] and at the edge of a homogeneous plate [11]. Truncation of the problem domain and the imposition of additional boundary conditions has the effect of imposing a periodic solution that approximates the corresponding unbounded domain field. However, the errors introduced in the vicinity of the scatterer can be made as small as desired by increasing the size of the unit cell of the periodic system to ensure that the artificial boundaries are far enough from the region of interest to make their influence on the local solution negligible. The truncation means that a field can be expressed in the form of series expansions rather than integral transforms and a solution found by manipulating matrix relationships between expansion coefficients. The series is limited to a finite number of terms to compute numerical results and although this leads to a further approximation, the series truncation errors are controlled by simply adjusting the number of terms to achieve a desired accuracy. In the next section, we outline the problem formulation in which the electromagnetic field is expressed in terms of transverse electric and transverse magnetic scalar potentials. The corresponding quasi-static scalar kernels are derived in series form for different configurations including a truncated penetrable quarter-space. The latter are then used to form a dyadic kernel which guarantees that the solution of the electric field integral equation for the flaw field will satisfy the correct continuity conditions at the intersecting surfaces forming a right-angled wedge. A basic application of the moment method gives the flaw signals which are validated by comparison with measurements on notches. Finally, the conclusions are summarized with reference to the prospects for future developments.

## II. Formulation

### A. Outline of Problem

In the problem considered, a crack lies in a plane mutually perpendicular to and bounded by the horizontal and vertical

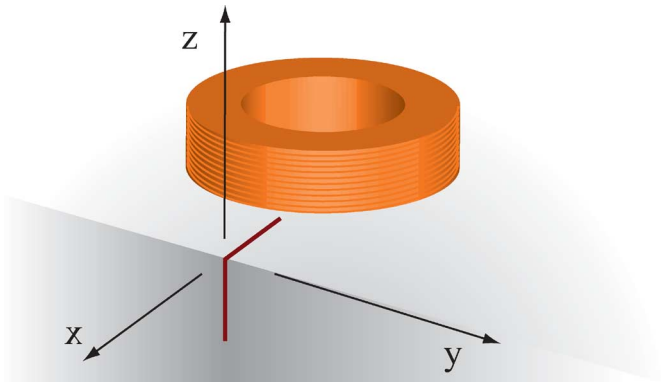


Fig. 1. Edge crack in a plane mutually perpendicular to surfaces of a right-angled conductive wedge.

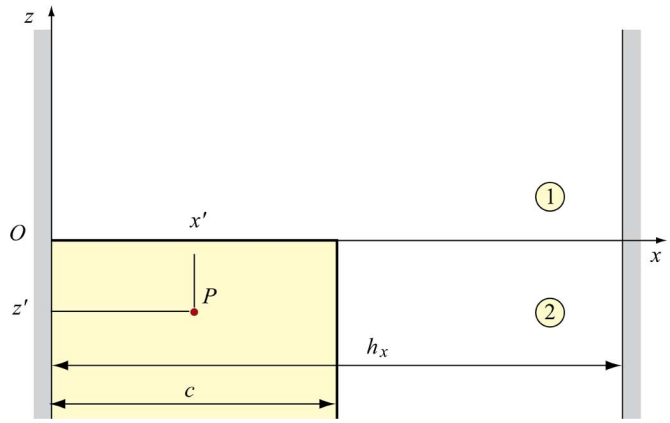


Fig. 2. Singular source at P in truncated conductive quarter-space.

faces of a conductive quarter-space; see Fig. 1. An induction coil whose axis is normal to the horizontal surface of the conductor carries an alternating current and thereby interacts inductively with the cracked conductor. In our preliminary work, the coil impedance as a function of position with respect to the edge of a homogeneous (flawless) quarter-space was determined using an eigenfunction expansion of the truncated domain solution [9]. Good agreement with experiment was obtained with this approach by using a series solution with just 40 terms. The induced current density in a flawless quarter-space conductor due to a coil has also been determined [10]. In effect, this is the incident field for the present problem.

To derive the required kernel for a quarter-space, we use a Cartesian coordinate system, Fig. 2, with the $y$-axis parallel with the edge of a right-angled conductive wedge and the edge is at $x = c$. Later, when we compare theory and experiment we shall refer to the coordinate system in Fig. 1 with the origin at the midpoint of the edge. For the field calculation, the domain of the problem is restricted in the $x$ direction to a region between $x = 0$ and $x = h_x$ with one wedge face at the half plane $x = c$, $z < 0$. The other face is in the plane $z = 0$ and limited to $0 \leq x \leq c$. The problem region is also truncated in the $y$-direction with truncation boundaries at $y = 0$ and $y = h_y$. Truncation in $y$ is not essential but prepares the way for an efficient numerical implementation using Fourier series. On the boundaries formed by domain truncation, we assume either that the tangential electric field is zero or that the tangential magnetic field is zero. These are referred to as a perfect electrical conductor (PEC) boundary condition and a perfect magnetic conductor (PMC) boundary condition, respectively. Boundary conditions for the present problem are summarized in Table I. They are nominal in the sense that they are imposed at remote locations where the field is in fact negligible compared with that close to the primary source. The choices reflect a desire to keep the series expansions as simple as possible.

TABLE I
TRUNCATION BOUNDARY CONDITIONS

| Plane | Field | Transverse Potential |
|---|---|---|
| $x = 0$ | $\hat{x} \times \boldsymbol{E} = 0$ | $W_a = 0 \quad \frac{\partial W_b}{\partial x} = 0$ |
| $x = h_x$ | $\hat{x} \times \boldsymbol{H} = 0$ | $\frac{\partial W_a}{\partial x} = 0 \quad W_b = 0$ |
| $y = 0$ | $\hat{y} \times \boldsymbol{H} = 0$ | $W_a = 0 \quad \frac{\partial W_b}{\partial y} = 0$ |
| $y = h_y$ | $\hat{y} \times \boldsymbol{E} = 0$ | $\frac{\partial W_a}{\partial y} = 0 \quad W_b = 0$ |

### B. Scalar Decomposition

We express the time-harmonic magnetic field, varying at an angular frequency $\omega$ as the real part of $\exp(-\imath\omega t)$, in terms of second order potentials

$$\boldsymbol{H} = \nabla \times \nabla \times \mathbf{W} \quad \text{with} \quad \mathbf{W} = \hat{x}W_a + \nabla \times (\hat{x}W_b) \tag{1}$$

where $\hat{x}$ is a unit vector. Let $W$ refer to either the transverse electric potential $W_a$ or the transverse magnetic potential $W_b$. Using the transverse gradient $\nabla_t = \nabla - \hat{x}(\partial/\partial x)$, the TE and TM potentials satisfy

$$\nabla^2 \nabla_t^2 W = 0 \tag{2}$$

for the field in air (we refer to the field arising from eddy currents in the wedge and not to the field from the driver coil). For the conductive region, the potential satisfies the modified Helmholtz equation

$$(\nabla^2 + k^2)\nabla_t^2 W = 0 \tag{3}$$

where $k^2 = i\omega\mu_0\mu_r\sigma_0$ with $\sigma_0$ denoting the conductivity, $\mu_0$ and $\mu_r$ the vacuum and relative magnetic permeabilities, respectively. For reference, the following expressions for the electromagnetic field are given. Firstly, the magnetic field is expressed as

$$\boldsymbol{H} = \nabla \times \nabla \times (\hat{x}W_a) + k^2 \nabla \times (\hat{x}W_b) \tag{4}$$

and the components of the magnetic field are therefore

$$H_x = -\nabla_t^2 W_a \tag{5}$$

$$H_y = \frac{\partial^2 W_a}{\partial x \partial y} + k^2 \frac{\partial W_b}{\partial z} \tag{6}$$

and

$$H_z = \frac{\partial^2 W_a}{\partial x \partial z} - k^2 \frac{\partial W_b}{\partial y}. \tag{7}$$

The electric field in source-free regions is given by

$$\boldsymbol{E} = i\omega\mu \left[\nabla \times (\hat{x} W_a) + \nabla \times \nabla \times (\hat{x} W_b)\right] \tag{8}$$

and its components are therefore

$$E_x = -i\omega\mu \nabla_t^2 W_b \tag{9}$$

$$E_y = i\omega\mu \left( \frac{\partial W_a}{\partial z} + \frac{\partial^2 W_b}{\partial x \partial y} \right) \tag{10}$$

and

$$E_z = -i\omega\mu \left( \frac{\partial W_a}{\partial y} - \frac{\partial^2 W_b}{\partial x \partial z} \right). \tag{11}$$

By using a scalar decomposition with $x$ as the preferred direction, Fig. 2, and selecting the truncation boundary condition judiciously we have avoided coupling of the TE and TM modes at the $x = c$ surface.[1] At the $z = 0$ plane, however, mode coupling is unavoidable. This implies that a TE field which migrates upward to interact with the field in the upper region at the plane $z = 0$ will give rise to both TE and TM fields, partially transmitted through the surface and partially reflected. Furthermore, we note that the $z = 0$ interface is divided at $x = c$ by the edge of the truncated quarter-space. Consequently, a field component of a given spatial frequency defined with respect to the $x$ direction will couple with terms of all other spatial frequencies associated with the field variation in $x$. Thus mode coupling takes place in two forms at the $z = 0$ plane. It couples the TE and TM modes and it couples terms in the Fourier series expansions with respect to $x$ whose spatial frequencies are different as well as those which are the same. Clearly, the solution must take account of these effects.

### C. Scalar Green's Functions

In order to construct the required dyadic kernel we first introduce scalar Green's functions that embody the effects of interface coupling between the transverse modes. These include the function $G_{aa}(\boldsymbol{r}|\boldsymbol{r}')$ representing a TE potential due to a TE source and $G_{ab}(\boldsymbol{r}|\boldsymbol{r}')$ representing a TE mode emanating from the $z = 0$ interface by mode coupling from a TM source, similarly for the TM mode. Thus, to determine solutions of the field equations, we define a Green's function satisfying

$$\nabla^2 \begin{bmatrix} G_{aa} & G_{ab} \\ G_{ba} & G_{bb} \end{bmatrix} = \begin{bmatrix} 0 & 0 \\ 0 & 0 \end{bmatrix} \tag{12}$$

for the external region and

$$(\nabla^2 + k^2) \begin{bmatrix} G_{aa} & G_{ab} \\ G_{ba} & G_{bb} \end{bmatrix} = -\delta(\boldsymbol{r} - \boldsymbol{r}') \begin{bmatrix} 1 & 0 \\ 0 & 1 \end{bmatrix} \tag{13}$$

[1]With the same preferred direction, a different set of boundary conditions can give rise to mode coupling for zero order terms in a series expansion of the TM potential; see [9].

for the conductive region. In addition, it is convenient to define functions $U_{aa}(\boldsymbol{r}|\boldsymbol{r}')$, etc. called the integrated kernels, such that

$$\begin{bmatrix} G_{aa} & G_{ab} \\ G_{ba} & G_{bb} \end{bmatrix} = -\nabla_t^2 \begin{bmatrix} U_{aa} & U_{aa} \\ U_{ba} & U_{bb} \end{bmatrix}. \tag{14}$$

Because $W_a$ satisfies a modified Helmholtz equation (3), with transverse Laplace operator $\nabla_t^2$, the integrated kernel $U_{aa}(\boldsymbol{r}|\boldsymbol{r}')$ is identified as a TE potential due to a TE delta function source, whereas $U_{ab}(\boldsymbol{r}|\boldsymbol{r}')$ is also a TE potential but arises from a TM source via mode coupling at an interface. Similarly, $U_{ba}(\boldsymbol{r}|\boldsymbol{r}')$ and $U_{bb}(\boldsymbol{r}|\boldsymbol{r}')$ are identified with the TM potential due to a delta function source.

### D. Dyadic Kernel

The scalar Green's functions have been determined in series form and then used to construct a dyadic Green's function for generating the electric field from an electric source in the conductor. The aim is to find solutions of Maxwell's equations in the quasi-static limit for an internal induced electric dipole density $\boldsymbol{P}(\boldsymbol{r}) = [\sigma(\boldsymbol{r}) - \sigma_0]\boldsymbol{E}(\boldsymbol{r})$, representing the effect of a flaw in a material whose permeability is that of free space and whose conductivity $\sigma(\mathrm{r})$, which differs from that of the host conductivity $\sigma_0$ in the flaw region. The linear quasi-static field equations with the electric source $\boldsymbol{P}(\boldsymbol{r})$

$$\nabla \times \boldsymbol{E}(\boldsymbol{r}) = \imath\omega\mu_0 \boldsymbol{H}(\boldsymbol{r}) \tag{15}$$

and

$$\nabla \times \boldsymbol{H}(\boldsymbol{r}) = \sigma_0 \boldsymbol{E}(\boldsymbol{r}) + \boldsymbol{P}(\boldsymbol{r}) \tag{16}$$

have a solution that can be found from an integral equation which expresses the electric field as the sum of an incident field $\boldsymbol{E}^{(i)}(\boldsymbol{r})$ and a field due to the presence of a flaw [2]

$$\boldsymbol{E}(\boldsymbol{r}) = \boldsymbol{E}^{(i)}(\boldsymbol{r}) + i\omega\mu_0 \int_{\Omega_0} \mathcal{G}(\boldsymbol{r}|\boldsymbol{r}') \cdot \boldsymbol{P}(\boldsymbol{r}') d\boldsymbol{r}' \tag{17}$$

where $\Omega_0$ is the domain of the flaw and $\mathcal{G}(\boldsymbol{r}|\boldsymbol{r}')$ is a dyadic Green's function for transforming an electric source in a conductive region into an electric field. The quarter-space dyadic kernel $\mathcal{G}(\boldsymbol{r}|\boldsymbol{r}')$ can be expressed in terms of $U_{aa}(\boldsymbol{r}|\boldsymbol{r}')$, $U_{ab}(\boldsymbol{r}|\boldsymbol{r}')$, $U_{ba}(\boldsymbol{r}|\boldsymbol{r}')$, and $U_{bb}(\boldsymbol{r}|\boldsymbol{r}')$ using a generalization [12] of the corresponding expressions in the absence of mode coupling [13].

Once the dipole density is computed, the coil impedance change due to the flaw $\Delta Z$ can be calculated by using the reciprocity theorem as follows: [2]

$$I^2 \Delta Z = -\int_{\Omega_0} \boldsymbol{E}^{(i)}(\boldsymbol{r}) \cdot \boldsymbol{P}(\boldsymbol{r}) d\boldsymbol{r}. \tag{18}$$

### E. Scalar Mode Coupling

Before entering unfamiliar territory it is often helpful to become further acquainted with its more easily recognizable features. Likewise, before considering the dyadic kernel for the

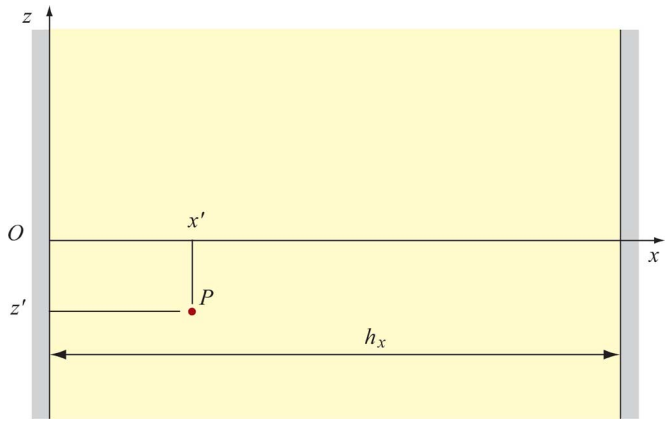


Fig. 3. Singular source at P in a truncated homogeneous conductive region.

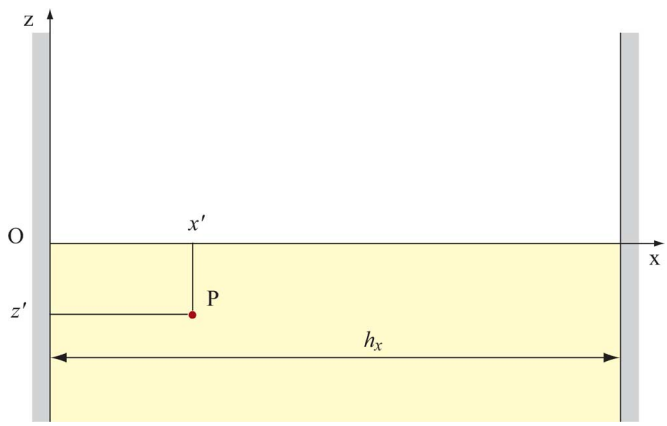


Fig. 4. Singular source at P in a conductive region below a plane surface above which is a nonconductive region.

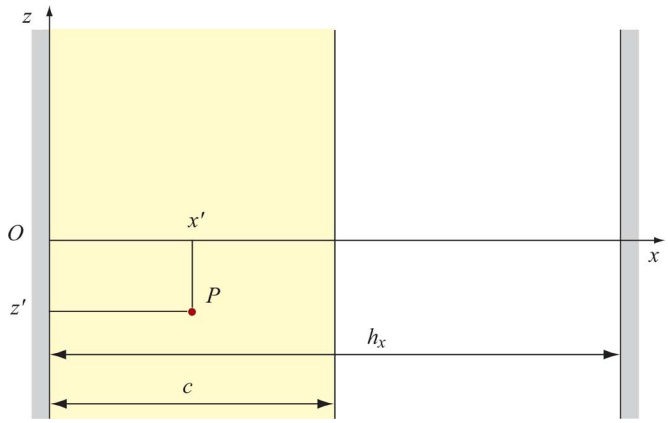


Fig. 5. Singular source at P in a conductive region $x \leq c$ adjacent to a nonconductive region ($c \leq x \leq h_x$).

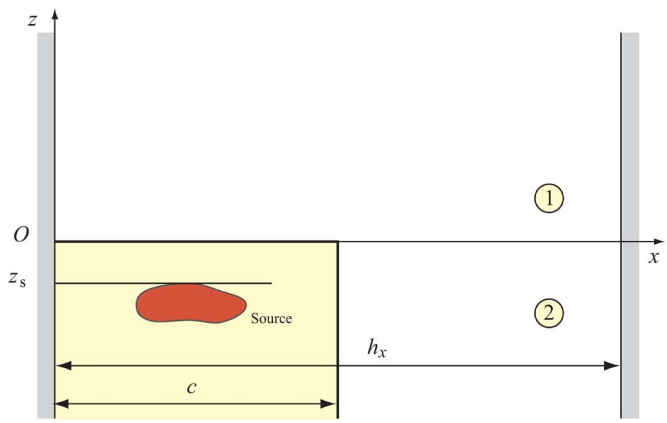


Fig. 6. Arbitrary source in a bitruncated quarter-space.

corner crack problem, some simpler results will be examined to set the quarter-space analysis in context. We therefore examine first singular sources in uniform domains truncated in the $x$ and $y$ direction; see Fig. 3. Then compare these preliminary results with those for the case of a domain divided by a horizontal plane into conductive and nonconductive regions; see Fig. 4. The scalar decomposition throughout is with respect to the $x$-direction. Hence the preferred direction in the horizontally divided region is parallel to the surface of the conductor. As a result, TE and TM modes are coupled at the dividing plane. Eventually this bitruncated half-space configuration provides a useful link with the quarter-space solutions since it represents a limiting case of the latter in which $c \to h_x$; see Fig. 2. Next we determine scalar kernels for a vertically divided domain; see Fig. 5. In this case the preferred direction is normal to the interface and there is no coupling between TE and TM modes. Quarter-space scalar Green's functions are then expressed in terms of the corresponding kernels for the vertically divided domain plus terms representing field migration from the $z = 0$ plane. Having reached that point, we check consistency of the quarter-space results with the horizontally divided domain expressions in the limit as $c \to h_x$. Then the quarter-space dyadic kernel is assembled from its scalar modes.

## III. Scalar Kernels for Uniform Truncated Region

We seek first the transverse electric Green's function $G_a^{(0)}$ and the transverse magnetic Green's function $G_b^{(0)}$, defined with respect to the $x$-direction for a homogenous conductive truncated domain, with each scalar kernel arising from a corresponding singular source; see Fig. 3. Boundary conditions on $G_a^{(0)}$ are the same as those on $W_a$ and those on $G_b^{(0)}$ the same as those on $W_b$; see Table I.

A solution vanishing at $x = 0$ and at $y = 0$ can be expressed in terms of a sine series in both $x$ and $y$. Thus the TE solution of

$$(\nabla^2 + k^2)G^{(0)}(\boldsymbol{r}|\boldsymbol{r}') = -\delta(\boldsymbol{r} - \boldsymbol{r}') \tag{19}$$

can be written in the form

$$G_a^{(0)}(\boldsymbol{r}|\boldsymbol{r}') = \frac{4}{h_x h_y} \sum_{j=1}^{\infty} \sin(v_j y) \sin(v_j y') \times \sum_{i=1}^{\infty} \sin(u_i x) \sin(u_i x') \widetilde{G}(z, z', \lambda_{ij}). \tag{20}$$

The PMC boundary condition at $x = h_x$ is satisfied by making $u_i = (2i - 1)\pi/(2h_x)$ and the PEC condition at $y = h_y$ is satisfied by putting $v_j = (2j - 1)\pi/(2h_y)$. Substitute (20) into (13), multiply by $\sin(u_\ell x) \sin(v_m y)$, and integrate with respect

to $x$ between zero and $h_x$ and with respect to $y$ between zero and $h_y$, and we have that (20) satisfies (13) if

$$\left[\frac{\partial^2}{\partial z^2} - \lambda_{\ell m}^2\right] \widetilde{G}(z, z', \lambda_{\ell m}) = -\delta(z - z') \tag{21}$$

where $\lambda_{\ell m} = \sqrt{u_\ell^2 + v_m^2 - k^2}$. The solution of (21), continuous at $z'$ but with a discontinuity of $-1$ in the $z$-derivative, is simply

$$\widetilde{G}(z, z', \lambda_{\ell m}) = \frac{1}{2\lambda_{\ell m}} e^{-\lambda_{\ell m}|z - z'|}. \tag{22}$$

Equation (20) with (22) gives the TE Green's function for a homogeneous bitruncated domain. The TM Green's function, found in a similar way, is

$$G_b^{(0)}(\boldsymbol{r}|\boldsymbol{r}') = \frac{4}{h_x h_y} \sum_{j=1}^{\infty} \cos(v_j y) \cos(v_j y') \times \sum_{i=1}^{\infty} \cos(u_i x) \cos(u_i x') \widetilde{G}(z, z', \lambda_{ij}). \tag{23}$$

A Fourier series representation of the TE and TM kernels implies that the solution can be regarded as periodic in an extended infinite domain in which the singular source in a unit cell gives rise to a regularly spaced infinite sequence of images. A summation of contributions from the original source and its images provides an alternative expression to the Fourier series form for the truncated homogeneous domain kernels. Next we consider coupling between modes due to an interface at a horizontal plane.

## IV. Domain Divided Horizontally

### A. Arbitrary Source

Fig. 4 shows a truncated domain divided horizontally at $z = 0$. Rather than starting with a point source at P, we consider initially formal expressions for the scalar fields due to an arbitrary distributed source below the plane $z = z_s$ where $z_s < 0$. Later we examine the corresponding Green's functions for the TE and TM modes as a special case of the arbitrary source problem. In general, however, the TE potential has the form

$$W_a = \sum_{j=1}^{\infty} \sin(v_j y) \sum_{i=0}^{\infty} \sin(u_j x) \times \begin{cases} e^{-\kappa_{ij} z} C_{ij}^{(1)} & z > 0 \\ e^{-\lambda_{ij} z} C_{ij}^{(0)} + e^{\lambda_{ij} z} C_{ij}^{(2)} & 0 \geq z > z_s \end{cases} \tag{24}$$

where $\kappa_{ij} = \sqrt{u_i^2 + v_j^2}$ and the upper limit of the source region is at $z = z_s$. The coefficient $C_{ij}^{(0)}$ is associated with field migration from the source whereas $C_{ij}^{(1)}$ and $C_{ij}^{(2)}$ are associated, respectively, with transmission and reflection at the interface. The TM solution for the region of the conductor where $z_s < z \leq 0$ can be written

$$W_b = \sum_{j=1}^{\infty} \cos(v_j y) \sum_{i=1}^{\infty} \cos(u_i x) \left(e^{-\lambda_{ij} z} D_{ij}^{(0)} + e^{\lambda_{ij} z} D_{ij}^{(2)}\right). \tag{25}$$

Coefficient $D_{ij}^{(0)}$ is associated with field migration from the source and $D_{ij}^{(2)}$ with migration from the interface. The expansion coefficients, being linearly related, can be written in terms of transmission and reflection coefficients

$$\begin{bmatrix} C_{ij}^{(1)} \\ D_{ij}^{(1)} \end{bmatrix} = \begin{bmatrix} T_{ij}^{(aa)} & T_{ij}^{(ab)} \\ T_{ij}^{(ba)} & T_{ij}^{(bb)} \end{bmatrix} \begin{bmatrix} C_{ij}^{(0)} \\ D_{ij}^{(0)} \end{bmatrix} \tag{26}$$

and

$$\begin{bmatrix} C_{ij}^{(2)} \\ D_{ij}^{(2)} \end{bmatrix} = \begin{bmatrix} R_{ij}^{(aa)} & R_{ij}^{(ab)} \\ R_{ij}^{(ba)} & R_{ij}^{(bb)} \end{bmatrix} \begin{bmatrix} C_{ij}^{(0)} \\ D_{ij}^{(0)} \end{bmatrix} \tag{27}$$

which are determined by the field continuity conditions for the $z = 0$ interface. The continuity of $H_x$, $H_y$ and $B_z$ are ensured, in the weak sense, by enforcing continuity of moments of the field components. This is done by having

$$\int_0^{h_y} \sin(v_m y) \int_0^{h_x} \sin(u_\ell x) H_x dx dy$$

$$\int_0^{h_y} \cos(v_m y) \int_0^{h_x} \cos(u_\ell x) H_y dx dy$$

and

$$\int_0^{h_y} \sin(v_m y) \int_0^{h_x} \cos(u_\ell x) B_z dx dy$$

are continuous at $z = 0$ for all $\ell$ and $m$. Using the continuity conditions gives, respectively

$$u_i^2 C_{ij}^{(1)} = \left(u_i^2 - k^2\right)\left(C_{ij}^{(0)} + C_{ij}^{(2)}\right) \tag{28}$$

$$u_i v_j C_{ij}^{(1)} = u_i v_j \left(C_{ij}^{(0)} + C_{ij}^{(2)}\right) - k^2 \lambda_{ij} \left(D_{ij}^{(0)} - D_{ij}^{(2)}\right) \tag{29}$$

and

$$\kappa_{ij} u_i C_{ij}^{(1)} = \mu_r u_i \lambda_{ij} \left(C_{ij}^{(\mathrm{H})} - C_{ij}^{(2)}\right) - \mu_r k^2 v_j \left(D_{ij}^{(0)} + D_{ij}^{(2)}\right) \tag{30}$$

from which the reflection coefficients are found to be

$$R_{ij}^{(aa)} = \frac{\mu_r \left(\lambda_{ij}^2 u_i^2 + k^2 v_j^2\right) - \kappa_{ij} \lambda_{ij} \left(u_i^2 - k^2\right)}{\kappa_{ij} (\lambda_{ij} + \mu_r \kappa_{ij}) \left(u_i^2 - k^2\right)} \tag{31}$$

$$R_{ij}^{(ab)} = -\frac{2\mu_r k^2 \lambda_{ij} u_i v_j}{\kappa_{ij} (\lambda_{ij} + \mu_r \kappa_{ij}) \left(u_i^2 - k^2\right)} \tag{32}$$

$$R_{ij}^{(ba)} = -\frac{2\mu_r \lambda_{ij} u_i v_j}{\kappa_{ij} (\lambda_{ij} + \mu_r \kappa_{ij}) \left(u_i^2 - k^2\right)} \tag{33}$$

and

$$R_{ij}^{(bb)} = \frac{\mu_r\left(\lambda_{ij}^2 u_i^2 + k^2 v_j^2\right) + \kappa_{ij}\lambda_{ij}\left(u_i^2 - k^2\right)}{\kappa_{ij}(\lambda_{ij} + \mu_r\kappa_{ij})\left(u_i^2 - k^2\right)}. \tag{34}$$

Defining

$$\Delta_{ij} = \kappa_{ij}(\lambda_{ij} + \mu_r\kappa_{ij})\left(u_i^2 - k^2\right) \tag{35}$$

these relationships can be written succinctly as

$$\begin{bmatrix} R_{ij}^{(aa)} + 1 & R_{ij}^{(ab)} \\ R_{ij}^{(ba)} & R_{ij}^{(bb)} - 1 \end{bmatrix} = \frac{2\mu_r}{\Delta_{ij}} \begin{bmatrix} \lambda_{ij}^2 u_i^2 & -k^2\lambda_{ij}u_i v_j \\ -\lambda_{ij}u_i v_j & k^2 v_j^2 \end{bmatrix}. \tag{36}$$

The interface coefficients are next used in constructing the divided domain Green's functions.

### B. Singular Sources

In the case of truncated half-space solution for point sources, $W_a$ can be identified with $U_{aa}$ if it originates at a TE source and with $U_{ab}$ if it arises from a TM source. Similarly $W_b$ can be identified with $U_{ba}$ and $U_{bb}$. Thus comparing (19), (20), and (23) with (3), (24), and (25), one concludes that for a singular source at $\{x', y', z'\}$ $(0 \geq z > z')$

$$\begin{bmatrix} C_{ij}^{(0)} \\ D_{ij}^{(0)} \end{bmatrix} = -\frac{2}{h_x h_y} \begin{bmatrix} \sin(v_j y')\sin(u_i x') \\ \cos(v_j y')\cos(u_i x') \end{bmatrix} \frac{e^{\lambda_{ij} z'}}{\lambda_{ij}\left(u_i^2 - k^2\right)}. \tag{37}$$

It follows that the modal Green's functions for the horizontally divided domain are

$$\begin{aligned} \begin{bmatrix} G_{aa}^{(\mathrm{H})} & G_{ab}^{(\mathrm{H})} \\ G_{ba}^{(\mathrm{H})} & G_{bb}^{(\mathrm{H})} \end{bmatrix} &= \frac{4}{h_x h_y} \\ &\begin{bmatrix} \sum_{j=1}^{\infty}\sin(v_j y)\sum_{i=1}^{\infty}\sin(u_i x) & 0 \\ 0 & \sum_{j=1}^{\infty}\cos(v_j y)\sum_{i=1}^{\infty}\cos(u_i x) \end{bmatrix} \\ &\times \begin{bmatrix} \tilde{g}_{ij}^{(aa)} & \tilde{g}_{ij}^{(ab)} \\ \tilde{g}_{ij}^{(ba)} & \tilde{g}_{ij}^{(bb)} \end{bmatrix} \\ &\times \begin{bmatrix} \sin(v_j y')\sin(u_i x') & 0 \\ 0 & \cos(v_j y')\cos(u_i x') \end{bmatrix} \end{aligned} \tag{38}$$

where

$$\begin{bmatrix} \tilde{g}_{ij}^{(aa)} & \tilde{g}_{ij}^{(ab)} \\ \tilde{g}_{ij}^{(ba)} & \tilde{g}_{ij}^{(bb)} \end{bmatrix} = \frac{1}{2\lambda_{ij}} \left\{ \begin{bmatrix} 1 & 0 \\ 0 & 1 \end{bmatrix} e^{-\lambda_{ij}|z-z'|} + \begin{bmatrix} R_{ij}^{(aa)} & R_{ij}^{(ab)} \\ R_{ij}^{(ba)} & R_{ij}^{(bb)} \end{bmatrix} e^{\lambda_{ij}(z+z')} \right\}. \tag{39}$$

It is of passing interest that the scalar kernels for the truncated half-space can be used to construct a dyadic kernel for solving scattering problem of a flaw in a half-space conductor. In the case of an infinitesimally thin crack in a $yz-$ plane, only the TM mode is perturbed by the defect and the scattering problem could therefore be formulated only in terms of the TM mode. However, this is not a line of enquiry we pursue here.

Fourier coefficients in two dimensions have been matched across the horizontal interface in order to get expressions for the scalar kernels in a bitruncated half-space with the results expressed above in the form of a double series. In the case of the quarter-space problem, in contrast, Fourier components defined with respect to the $x$-direction do not match on a term-by-term basis across the plane $z = 0$ because of the nonuniformity of the horizontal interface. Instead there is coupling between Fourier components containing $u_i$ and $u_\ell$ $(i \neq \ell)$ for example, with triple series expressions for the kernels to account for it. Before dealing with mode coupling at a divided interface, we consider next a simple case, that of a vertically divided domain.

## V. Vertically Divided Domain

### A. TE Mode

For the TE mode in a bitruncated domain divided at a vertical interface at the plane $x = c$, Fig. 5, we form a solution

$$\begin{aligned} G_a^{(\mathrm{V})} = &\sum_{j=1}^{\infty}\sin(v_j y)\sin(v_j y') \times \sum_{i=1}^{\infty}\sin(q_i x) \\ &\times \begin{cases} \sin(q_i x)e^{-\gamma_{ij}|z-z'|}A_{ij} & 0 \leq x < c \\ \cos\left[p_i(h_x - x)\right]e^{-\gamma_{ij}|z-z'|}\alpha_i A_{ij} & c \leq x < h_x \end{cases} \end{aligned} \tag{40}$$

where $p_i = \sqrt{q_i^2 - k^2}$, $\gamma_{ij} = \sqrt{q_i^2 + v_j^2 - k^2}$ and the $q_i$ eigenvalues are determined from the continuity of the normal magnetic flux density and tangential magnetic field at the $x = c$ interface. The continuity of $B_x$ at $x = c$ implies that

$$\mu_r \sin(q_i c) = \alpha_i \cos\left[p_i\left(h_x - c\right)\right] \tag{41}$$

whereas the continuity of $\boldsymbol{H}_t$ at the $x = c$ implies that

$$q_i \cos(q_i c) = \alpha_i p_i \sin\left[p_i(h_x - c)\right]. \tag{42}$$

The values of $q_i$ and hence $p_i$ are sought using (41) and (42). Eliminating $\alpha_i$, one finds the values of $q_i$ from the roots of

$$\begin{aligned} 0 = &\, q_i \cos q_i c \cos\left[\sqrt{q_i^2 - k^2}(h_x - c)\right] \\ &-\mu_r\sqrt{q_i^2 - k^2}\sin q_i c \sin\left[\sqrt{q_i^2 - k^2}(h_x - c)\right]. \end{aligned} \tag{43}$$

The roots can be found using an algorithm which systematically searches the complex plane for the zeros of a function [10], [14]–[16]. The coefficients in (40) are determined by using a set of eigenfunctions defined by

$$\psi_\ell(x) = \begin{cases} \sin(q_\ell x) & 0 \leq x < c \\ \frac{\alpha_\ell}{\sqrt{\mu_r}}\cos\left[p_\ell(h_x - x)\right] & c \leq x < h_x \end{cases} \tag{44}$$

and having the orthogonal property

$$\int_0^{h_x} \psi_i(x)\psi_j(x)dx = \frac{h_i}{2}\delta_{ij} \tag{45}$$

where

$$h_i = \frac{\alpha_i^2}{\mu_r}(h_x - c) + \left[c + \frac{k^2}{p_i^2}\frac{\sin(2q_i c)}{2q_i}\right]. \tag{46}$$

By substituting (40) into (12) and (13), using (44)–(46) and the orthogonality property of $\sin v_j y$ to determine $A_{ij}$, one finds that

$$G_a^{(\mathrm{V})}=\frac{4}{h_y}\sum_{j=1}^{\infty}\sin(v_j y)\sin(v_j y') \times\begin{cases}\sum\limits_{i=1}^{\infty}\frac{1}{h_i}\sin(q_i x)\sin(q_i x')\widetilde{G}(z,z',\gamma_{ij}) & 0\le x\le c\\ \sum\limits_{i=1}^{\infty}\frac{1}{h_i}\cos[p_i(h_x-x)]\sin(q_i x')\alpha_i\widetilde{G}(z,z',\gamma_{ij}) & c<x\le h_x\end{cases} \tag{47}$$

where $\widetilde{G}(z,z',\gamma_{ij})$ is given by (22). Hence the Green's function for the conductive region has the same general form as that for a homogeneous truncated domain. However, complex series coefficients $h_i$ now replace the domain dimension $h_x$ and the complex eigenvalues $q_i$ replace the real values denoted by $u_i$.

### B. TM Mode

The TM Green's kernel for the vertically divided truncated domain takes the form

$$G_b^{(\mathrm{V})}=\frac{4}{ch_y}\sum_{j=1}^{\infty}\cos(v_j y)\cos(v_j y') \times\sum_{i=1}^{\infty}\cos(r_i x)\cos(r_i x')e^{-s_{ij}|z-z'|}B_{ij}\quad 0\le x\le c \tag{48}$$

where $s_{ij}=\sqrt{r_i^2+v_j^2-k^2}$. The TM kernel satisfies the condition that $\partial G_b^{(\mathrm{V})}/\partial x=0$ for $x=0$, ensuring that the tangential component of the electric field on the truncation boundaries is zero. The continuity of the tangential magnetic field at the air-conductor interface implies that $G_b^{(\mathrm{V})}=0$ at $x=c_-$, where the subscript refers to the limiting value as the boundary is approached from the conductive side. Putting $r_i=(2i-1)\pi/(2c)$ satisfies this condition. To find the expansion coefficients, one substitutes (48) into (13), multiplies by $\cos(r_\ell x)\cos(v_m y)$ and integrates with respect to $x$ from zero to $c$ and with respect to $y$ from zero to $h_y$ with $0\le x'\le c$, to give

$$G_b^{(\mathrm{V})}=\frac{4}{ch_y}\sum_{j=1}^{\infty}\cos(v_j y)\cos(v_j y') \times\sum_{i=1}^{\infty}\cos(r_i x)\cos(r_i x')\widetilde{G}(z,z',s_{ij})\quad 0\le x<c. \tag{49}$$

This completes the derivation of the decoupled modal Green's functions for the vertically divided domain. To define truncated quarter-space kernels, (47) and (49) are modified by adding the effect of field migration from an interface at the plane $z=0$. This has been done by first defining a set of transmission and reflection coefficients for TE and TM potentials due to an arbitrary source in the conductor.

## VI. Quarter-Space Solutions

### A. Arbitrary Source

We derive the Green's function for a source in a quarter-space by first deriving interface transmission and reflection coefficients needed for these kernels. Consider, therefore, an arbitrary source distribution in the conductor below a plane $z=z_s$ (Fig. 2), either an electric or magnetic dipole distribution or a combination of both. As in the case of a vertically divided domain, the field in the conductor is matched with the field in air across the vertical boundary in the plane $x=c$. In addition, the field in the region $(z_s<z\le 0)$ is matched with the field in the upper region of the problem domain $(z>0)$ across the horizontal boundary at $z=0$. We begin by noting the scalar modes in the different regions of the arbitrary source problem. The TE potential for the region above the $z=0$ plane can be expressed, as in (24), in

$$W_a=\sum_{j=1}^{\infty}\sin(v_j y)\sum_{i=1}^{\infty}\sin(u_i x)e^{-\kappa_{ij}z}C_{ij}^{(1)} \tag{50}$$

where $\kappa_{ij}=(u_i^2+v_j^2)^{1/2}$. For the region $z_s<z\le 0$, that is, below the upper surface of the conductor but above the source, the TE potential has the form

$$W_a=\sum_{j=1}^{\infty}\sin(v_j y) \times\begin{cases}\sum\limits_{i=1}^{\infty}\sin(q_i x)\left(e^{-\gamma_{ij}z}C_{ij}^{(\mathrm{V})}+e^{\gamma_{ij}z}C_{ij}^{(2)}\right) & 0\le x\le c,\\ \sum\limits_{i=1}^{\infty}\cos[p_i(h_x-x)]\alpha_i\left(e^{-\gamma_{ij}z}C_{ij}^{(\mathrm{V})}+e^{\gamma_{ij}z}C_{ij}^{(2)}\right) & c\le x<h_x\end{cases} \tag{51}$$

where the superscript V indicates that the coefficient is predetermined by satisfying the vertically divided domain interface conditions. The TM solution for the region of the conductor above the source can be written as

$$W_b=\sum_{j=1}^{\infty}\cos(v_j y)\sum_{i=1}^{\infty}\cos(r_i x)\left(e^{-s_{ij}z}D_{ij}^{(\mathrm{V})}+e^{s_{ij}z}D_{ij}^{(2)}\right) \tag{52}$$

for $z_s<z\le 0$ and $0\le x<c$. The unknown coefficients, $C_{ij}^{(1)}$, $C_{ij}^{(2)}$, and $D_{ij}^{(2)}$, are found by enforcing the continuity of the tangential magnetic field and the normal magnetic flux density at air-conductor interfaces.

### B. Formal Solution

The coefficients $C_{\ell j}^{(\mathrm{V})}$ and $D_{\ell j}^{(\mathrm{V})}$ are determined by the solution of the corresponding vertically divided domain problem for a given source. With these coefficients prescribed for the

quarter-space problem, the remaining coefficients, being linearly dependent on those for the vertically divided domain, can be expressed in the form

$$\begin{bmatrix} C_{ij}^{(1)} \\ D_{ij}^{(1)} \end{bmatrix} = \sum_{\ell=1}^{\infty} \begin{bmatrix} T_{i\ell j}^{(aa)} & T_{i\ell j}^{(ab)} \\ T_{i\ell j}^{(ba)} & T_{i\ell j}^{(bb)} \end{bmatrix} \begin{bmatrix} C_{\ell j}^{(\mathrm{V})} \\ D_{\ell j}^{(\mathrm{V})} \end{bmatrix} \tag{53}$$

and

$$\begin{bmatrix} C_{ij}^{(2)} \\ D_{ij}^{(2)} \end{bmatrix} = \sum_{\ell=1}^{\infty} \begin{bmatrix} R_{i\ell j}^{(aa)} & R_{i\ell j}^{(ab)} \\ R_{i\ell j}^{(ba)} & R_{i\ell j}^{(bb)} \end{bmatrix} \begin{bmatrix} C_{\ell j}^{(\mathrm{V})} \\ D_{\ell j}^{(\mathrm{V})} \end{bmatrix} \tag{54}$$

where $j = 1, 2 \ldots R_{i\ell j}^{(aa)} R_{i\ell j}^{(ab)} R_{i\ell j}^{(ba)}$ and $R_{i\ell j}^{(bb)}$ are elements of reflection matrices. $T_{i\ell j}^{(aa)} T_{i\ell j}^{(ab)} T_{i\ell j}^{(ba)}$ and $T_{i\ell j}^{(bb)}$ are elements of transmission matrices. In constructing a Green's kernel for an internal scattering problem, only $C_{ij}^{(2)}$ and $D_{ij}^{(2)}$ are needed. These can be expressed as

$$\begin{bmatrix} \boldsymbol{C}_j^{(2)} \\ \boldsymbol{D}_j^{(2)} \end{bmatrix} = \begin{bmatrix} \mathbf{R}_{\mathbf{j}}^{(\mathbf{aa})} & \mathbf{R}_{\mathbf{j}}^{(\mathbf{ab})} \\ \mathbf{R}_{\mathbf{j}}^{(\mathbf{ba})} & \mathbf{R}_{\mathbf{j}}^{(\mathbf{bb})} \end{bmatrix} \begin{bmatrix} \boldsymbol{C}_j^{(\mathrm{V})} \\ \boldsymbol{D}_j^{(\mathrm{V})} \end{bmatrix} \tag{55}$$

where $\mathbf{R}_{\mathbf{j}}^{(\mathbf{aa})}$ etc., are matrices and $\boldsymbol{C}_j^{(\mathrm{V})}$ etc., are column vectors.

### C. Application of Interface Conditions

The coefficients in the forgoing expansions are determined using the interface conditions at the surface $z = 0$ which ensure the continuity of $H_x$, $H_y$ and $B_z$. These conditions, applied in the weak sense, as in Section IV, give, respectively

$$\mathbf{u^2} \boldsymbol{C}_j^{(1)} = \mathbf{M p^2} \left( \boldsymbol{C}_j^{(\mathrm{V})} + \boldsymbol{C}_j^{(2)} \right) \tag{56}$$

$$\begin{aligned} v_j \mathbf{u} \boldsymbol{C}_j^{(1)} = {} & v_j \mathbf{M_a q} \left( \boldsymbol{C}_j^{(\mathrm{V})} + \boldsymbol{C}_j^{(2)} \right) \\ & - k^2 \mathbf{M_b s_j} \left( \boldsymbol{D}_j^{(\mathrm{V})} - \boldsymbol{D}_j^{(2)} \right) \end{aligned} \tag{57}$$

and

$$\begin{aligned} \boldsymbol{\kappa_j} \mathbf{u} \boldsymbol{C}_j^{(1)} = {} & \mu_r \mathbf{M_a q} \boldsymbol{\gamma_j} \left( \boldsymbol{C}_j^{(\mathrm{V})} - \boldsymbol{C}_j^{(2)} \right) \\ & - \mu_r k^2 v_j \mathbf{M_b} \left( \boldsymbol{D}_j^{(\mathrm{V})} + \boldsymbol{D}_j^{(2)} \right). \end{aligned} \tag{58}$$

Matrices $\mathbf{M}$, $\mathbf{M_a}$ and $\mathbf{M_b}$ are defined in Appendix A. Matrices $\mathbf{u^2}, \mathbf{p^2}$, etc., are diagonal and contain the eigenvalues. Eliminating $\boldsymbol{C}_j^{(1)}$ from (57) and (58) gives the linear system

$$\mathbf{A_{11}} \boldsymbol{C}_j^{(2)} + \mathbf{A_{12}} \boldsymbol{D}_j^{(2)} = -\mathbf{A_{11}} \boldsymbol{C}_j^{(\mathrm{V})} + \mathbf{A_{12}} \boldsymbol{D}_j^{(\mathrm{V})} \tag{59}$$

$$\mathbf{A_{21}} \boldsymbol{C}_j^{(2)} + \mathbf{A_{22}} \boldsymbol{D}_j^{(2)} = -(\mathbf{A_{21}} + 2\mathbf{K}) \boldsymbol{C}_j^{(\mathrm{V})} - \mathbf{A_{22}} \boldsymbol{D}_j^{(\mathrm{V})} \tag{60}$$

from which $\boldsymbol{C}_j^{(2)}$ and $\boldsymbol{D}_j^{(2)}$ can be found. We have defined

$$\mathbf{A_{11}} = v_j \left( \mathbf{u M_a q} - \mathbf{M p^2} \right) \qquad \mathbf{A_{12}} = k^2 \mathbf{u M_b s_j} \tag{61}$$

$$\mathbf{A_{21}} = \mu_r \mathbf{u M_a q} \boldsymbol{\gamma_j} + \boldsymbol{\kappa}_j \mathbf{M p^2} \qquad \mathbf{A_{22}} = \mu_r k^2 v_j \mathbf{u M_b}$$

$$\mathbf{K} = -\mu_r \mathbf{u M_a q} \boldsymbol{\gamma}_j. \tag{62}$$

From $\mathbf{A_{21}} \mathbf{A_{11}^{-1}}$ (59), (60) we get

$$\boldsymbol{D}_j^{(2)} - \boldsymbol{D}_j^{(\mathrm{V})} = 2\mathbf{A^{-1}} \left[ \mathbf{K} \boldsymbol{C}_j^{(\mathrm{V})} + \mathbf{A_{22}} \boldsymbol{D}_j^{(\mathrm{V})} \right] \tag{63}$$

where

$$\mathbf{A} = \left[ \mathbf{A_{21}} \mathbf{A_{11}^{-1}} \mathbf{A_{12}} - \mathbf{A_{22}} \right] \tag{64}$$

and hence from (59)

$$\boldsymbol{C}_j^{(2)} + \boldsymbol{C}_j^{(\mathrm{V})} = -2\mathbf{A_{11}^{-1}} \mathbf{A_{12}} \mathbf{A^{-1}} \left[ \mathbf{K} \boldsymbol{C}_j^{(\mathrm{V})} + \mathbf{A_{22}} \boldsymbol{D}_j^{(\mathrm{V})} \right]. \tag{65}$$

Comparing (65) and (63) with (55) shows that the reflection matrices are given by

$$\begin{aligned} & \begin{bmatrix} \mathbf{R}_{\mathbf{j}}^{(\mathbf{aa})} + \mathbf{I} & \mathbf{R}_{\mathbf{j}}^{(\mathbf{ab})} \\ \mathbf{R}_{\mathbf{j}}^{(\mathbf{ba})} & \mathbf{R}_{\mathbf{j}}^{(\mathbf{bb})} - \mathbf{I} \end{bmatrix} \\ & \quad = 2 \begin{bmatrix} -\mathbf{A_{11}^{-1}} \mathbf{A_{12}} \mathbf{A^{-1}} \mathbf{K} & -\mathbf{A_{11}^{-1}} \mathbf{A_{12}} \mathbf{A^{-1}} \mathbf{A_{22}} \\ \mathbf{A^{-1}} \mathbf{K} & \mathbf{A^{-1}} \mathbf{A_{22}} \end{bmatrix} \end{aligned} \tag{66}$$

which agrees with (36) in the limit as $c \to h_x$.

### D. Quarter-Space Modal Green's Functions

The quarter-space scalar Green's functions can be expressed in terms of those for the vertically divided domain, $G_a^{(\mathrm{V})}$ and $G_b^{(\mathrm{V})}$, given in Section V, plus additional terms representing the field migration from the interface at the plane $z = 0$ containing the reflection matrices in (54) and (55). The decomposition is expressed as

$$\begin{bmatrix} G_{aa} G_{ab} \\ G_{ba} G_{bb} \end{bmatrix} = \begin{bmatrix} G_a^{(\mathrm{V})} & 0 \\ 0 & G_b^{(\mathrm{V})} \end{bmatrix} + \begin{bmatrix} G^{(aa)} G^{(ab)} \\ G^{(ba)} G^{(bb)} \end{bmatrix} \tag{67}$$

for the region $z < 0$ and we define integrate kernels for the reflection terms such that

$$\begin{bmatrix} G^{(aa)} G^{(ab)} \\ G^{(ba)} G^{(bb)} \end{bmatrix} = -\nabla_t^2 \begin{bmatrix} U^{(aa)} U^{(ab)} \\ U^{(ba)} U^{(bb)} \end{bmatrix}. \tag{68}$$

The Green's functions can be deduced from the results of the previous section by identifying $C_{\ell j}^{(\mathrm{V})}$ and $D_{\ell j}^{(\mathrm{V})}$ in the vertically divided domain problem for the case where sources are singular. A similar procedure was adopted in Section IV for finding the Green's functions for the horizontally divided domain. In making the assignment, one must be aware that the corresponding TE/TM potential for a point source is the integrated kernel. Hence, to identify $C_{\ell j}^{(\mathrm{V})}$, we operate on (51) with $-\nabla_t^2$ and compare the appropriate term for the conductive region with the corresponding one in (47). Similarly with (52) and (49), one identifies $D_{\ell j}^{(\mathrm{V})}$. In this way we assign

$$-\left(q_i^2 - k^2\right) C_{\ell j}^{(\mathrm{V})} = \frac{2}{h_y h_\ell} \sin(v_j y') \sin(q_\ell x') \frac{e^{\gamma_{\ell j} z'}}{\gamma_{\ell j}} \tag{69}$$

and

$$-\left(r_i^2 - k^2\right) D_{\ell j}^{(\mathrm{V})} = \frac{2}{c h_y} \cos(v_j y') \cos(q_\ell x') \frac{e^{s_{\ell j} z'}}{s_{\ell j}}. \tag{70}$$

Then from the terms in (51) and (52) representing field migration from the interface at $z = 0$, we have (71), as shown at the bottom of the page, which may be compared with the reflection terms in the horizontally divided domain problem; see (38) and (39).

### *E. Quarter-Space Dyadic Green's Function*

The dyadic Green's function in (17) for the bitruncated quarter space, expressed in terms of scalar modes taking account of mode coupling in the plane $z = 0$, is

$$\begin{aligned}\mathcal{G}(\boldsymbol{r}|\boldsymbol{r}') = {} & (\nabla \times \hat{x})(\nabla' \times \hat{x}) U_{aa}(\boldsymbol{r}|\boldsymbol{r}') \\ & + \frac{1}{k^2}(\nabla \times \hat{x})(\nabla' \times \nabla' \hat{x}) U_{ab}(\boldsymbol{r}|\boldsymbol{r}') \\ & + (\nabla \times \nabla \times \hat{x})(\nabla' \times \hat{x}) U_{ba}(\boldsymbol{r}|\boldsymbol{r}') \\ & + \frac{1}{k^2}(\nabla \times \nabla \times \hat{x})(\nabla' \times \nabla' \times \hat{x}) U_{bb}(\boldsymbol{r}|\boldsymbol{r}'). \quad (72)\end{aligned}$$

This is of the same general form as the quasi-static dyadic kernel representing a dipole source in a conductive region adjacent to an infinite circular cylindrical hole and may be derived in the same way [12].

For calculations on an ideal crack, in a plane mutually perpendicular to the surfaces of the quarter space (Fig. 1), only the component $G^{(yy)}(\boldsymbol{r}|\boldsymbol{r}') = \hat{y} \cdot \mathcal{G}(\boldsymbol{r}|\boldsymbol{r}') \cdot \hat{y}$ is needed. Operating on (72) to isolate this component yields

$$\begin{aligned}G_{yy}(\boldsymbol{r}|\boldsymbol{r}') = {} & \frac{\partial^2 U_{aa}(\boldsymbol{r}|\boldsymbol{r}')}{\partial z \partial z'} + \frac{1}{k^2}\frac{\partial^3 U_{ab}(\boldsymbol{r}|\boldsymbol{r}')}{\partial z \partial x' \partial y'} + \frac{\partial^3 U_{ba}(\boldsymbol{r}|\boldsymbol{r}')}{\partial x \partial y \partial z'} \\ & + \frac{1}{k^2}\frac{\partial^4 U_{bb}(\boldsymbol{r}|\boldsymbol{r}')}{\partial x \partial y \partial x' \partial y'}. \quad (73)\end{aligned}$$

Similarly, if the crack opening is small, one can neglect components of the induced dipole density at the crack other than the $y$-component and compute the response using $G_{yy}(\boldsymbol{r}|\boldsymbol{r}')$. Evaluating the terms in (73) using the decomposition given in (68) together with (71) gives

$$\begin{aligned}\frac{\partial^2 U^{(aa)}}{\partial z \partial z'} = {} & -\frac{2}{h_y}\sum_{j=1}^{\infty} \sin(v_j y)\sin(v_j y') \\ & \times \sum_{i=1}^{\infty} \sin(q_i x)\frac{\gamma_{ij} e^{\gamma_{ij} z}}{(q_i^2 - k^2)} \\ & \times \sum_{\ell=1}^{\infty} R_{i\ell j}^{(aa)} \sin(q_\ell x')\frac{e^{\gamma_{\ell j} z'}}{h_\ell} \quad (74)\end{aligned}$$

$$\begin{aligned}\frac{1}{k^2}\frac{\partial^3 U^{(ab)}}{\partial z \partial x' \partial y'} = {} & -\frac{2}{c h_y k^2}\sum_{j=1}^{\infty} v_j \sin(v_j y)\sin(v_j y') \\ & \times \sum_{i=1}^{\infty} \sin(q_i x)\frac{\gamma_{ij} e^{\gamma_{ij} z}}{(q_i^2 - k^2)} \\ & \times \sum_{\ell=1}^{\infty} R_{i\ell j}^{(ab)} \sin(r_\ell x')\frac{r_\ell e^{s_{\ell j} z'}}{s_{\ell j}} \quad (75)\end{aligned}$$

$$\begin{aligned}\frac{\partial^3 U^{(ba)}}{\partial x \partial y \partial z'} = {} & -\frac{2}{h_y}\sum_{j=1}^{\infty} v_j \sin(v_j y)\sin(v_j y') \\ & \times \sum_{i=1}^{\infty} \sin(r_i x)\frac{r_i e^{s_{ij} z}}{(r_i^2 - k^2)} \\ & \times \sum_{\ell=1}^{\infty} R_{i\ell j}^{(ba)} \sin(q_\ell x')\frac{e^{\gamma_{\ell j} z'}}{h_\ell} \quad (76)\end{aligned}$$

and

$$\begin{aligned}\frac{1}{k^2}\frac{\partial^4 U^{(bb)}}{\partial x \partial y \partial x' \partial y'} = {} & -\frac{2}{c h_y k^2}\sum_{j=1}^{\infty} v_j^2 \sin(v_j y)\sin(v_j y') \\ & \times \sum_{i=1}^{\infty} \sin(r_i x)\frac{r_i e^{s_{ij} z}}{(r_i^2 - k^2)} \times \sum_{\ell=1}^{\infty} R_{i\ell j}^{(bb)} \sin(r_\ell x')\frac{r_\ell e^{s_{\ell j} z'}}{s_{\ell j}}. \quad (77)\end{aligned}$$

The method of moments provides a means of converting the integral equation for the induced dipole density at the flaw into a matrix equation which can be solved to give an approximate solution in a discrete form. This has been done by approximating the flaw field using $N$ piecewise constant volume elements and the solution sought by using the fact that, in the quasi-static limit, the normal current at the surface of a crack is zero. Applying this condition at $N$ matching points on the crack surface each at the center of the face of a volume element in the form of a rectangular parallelepiped defines the matrix [4], [12]. Details of the incident field calculation for a coil near the edge of a truncated quarter space are given in [10].

## VII. Results and Validation

In order to test the theory and numerical predictions, impedance measurements have been carried out using two coils and two test pieces. Two aluminum blocks with edge notches were used, each in a plane mutually perpendicular to the intersecting surfaces forming the edge. The notches were made with Electrical Discharge Machining (EDM). Each block is sufficiently large compared with the coil and scan dimensions

$$\begin{aligned}\begin{bmatrix} G^{(aa)} & G^{(ab)} \\ G^{(ba)} & G^{(bb)} \end{bmatrix} = {} & \frac{2}{h_y}\begin{bmatrix} \sum_{j=1}^{\infty}\sin(v_j y)\sum_{i=1}^{\infty}\sin(q_i x)e^{\gamma_{ij} z} & 0 \\ 0 & \sum_{j=1}^{\infty}\cos(v_j y)\sum_{i=1}^{\infty}\cos(u_i x)e^{s_{ij} z} \end{bmatrix} \\ & \times \sum_{\ell=1}^{\infty}\begin{bmatrix} R_{i\ell j}^{(aa)} & R_{i\ell j}^{(ab)} \\ R_{i\ell j}^{(ba)} & R_{i\ell j}^{(bb)} \end{bmatrix}\begin{bmatrix} \sin(v_j y')\sin(u_i x')\frac{e^{\gamma_{ij} z'}}{h_\ell \gamma_{\ell j}} & 0 \\ 0 & \cos(v_j y')\cos(u_i x')\frac{e^{s_{\ell j} z'}}{c s_{\ell j}} \end{bmatrix} \quad (71)\end{aligned}$$

TABLE II
TEST PARAMETERS

| Coil | | Testpiece | |
|---|---|---|---|
| Inner radius, $r_1$ | 5.00 mm | Conductivity, $\sigma$ | $17.7 \pm 0.6$ MS/m |
| Outer radius, $r_2$ | 7.35 mm | Notch A face | $4.98 \times 5.00$ mm |
| Axial length, $l$ | 4.00 mm | Notch A width | 0.160 mm |
| Turns, $N$ | 1198 | | |
| Lift-off, $L$ | 0.05mm | | |

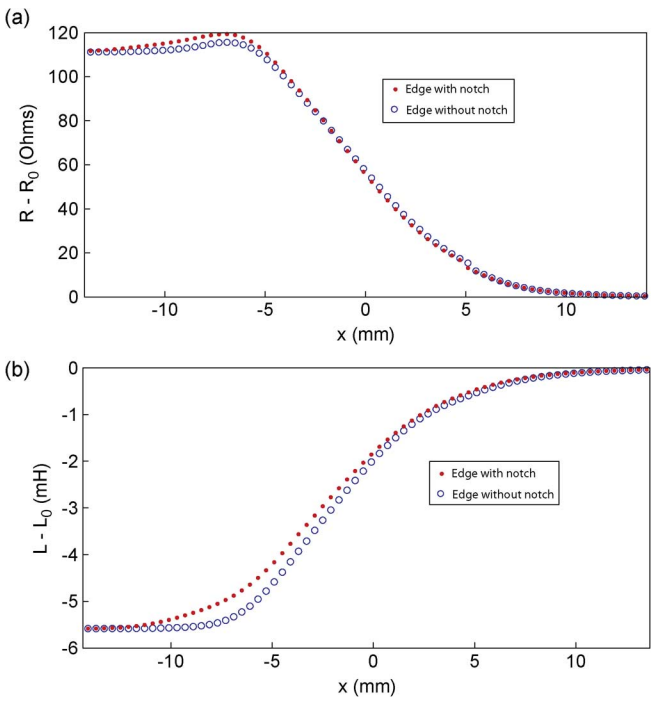


Fig. 7. Graphs show (a) resistance and (b) self-inductance variation of a coil with position as it passes over the edge of an aluminum block. Resistance and self-inductance values for the coil in air have been subtracted. Small filled circles show the calculated impedance variation when the axis of the coil is in the plane of an edge notch whereas the unfilled circles represent the corresponding calculated results without including the effect of the edge notch. Calculations assumed a frequency of 10 kHz and test parameters given in Table II.

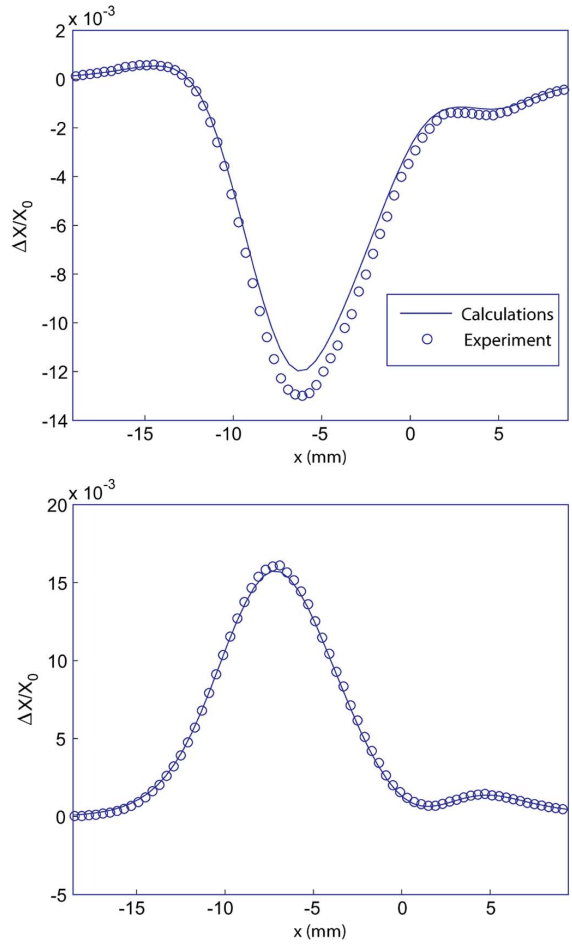


Fig. 8. Graphs show variation in resistance and reactance of an induction coil with position due to an edge notch. Results are normalized with respect to free space reactance of the coil. Experimental parameters are summarized in Table II. Coil is moved with it axis in the plane of the notch towards and over the edge while being excited at 1 kHz. Circles represent experimental data and solid line the calculated results.

TABLE III
TEST PARAMETERS

| Coil | | Testpiece | |
|---|---|---|---|
| Inner radius, $r_1$ | 5.00 mm | Conductivity, $\sigma$ | $17.0 \pm 0.6$ MS/m |
| Outer radius, $r_2$ | 9.7 mm | Notch B face | $10.0 \times 4.98$ mm |
| Axial length, $l$ | 4.00 mm | Notch B width | 0.175 mm |
| Turns, $N$ | 407 | | |
| Lift-off, $L$ | 1.08mm | | |

so that it can be represented as a conductive quarter-space. The coils were moved by a precision XY scanner (spatial resolution 0.025 mm) and measurements were made using the precision LCR bridge Agilent 4284A. The whole setup was PC controlled using Labview. We used two types of line scans in gathering the measurement data. In a crack scan the eddy current coil was moved along the notch and across the edge of the block, that is, in the $x$-direction shown by the coordinate system illustrated in Fig. 1. Crack scan measurements were performed using the test parameters in Table II. The coils are wound with a self-bonding wire and do not have a former. The block conductivity was measured using the conductivity mode of GE Phasec 2-D eddy current instrument. Calculated variations of the coil resistance and self-inductance with position at an edge near and away from the notch are shown in Fig. 7. The variation of the normalized resistance and reactance at 1 kHz due to the notch is displayed in Fig. 8, showing good agreement between theoretical predictions and experiment. The corresponding impedance plane display of the same data is shown in Fig. 9. Normalization is carried out by dividing by the free-space coil reactance $X_0$. A small discrepancy is observed in the real part of the impedance change and is attributed to measurement errors. It is also interesting to observe the relative magnitude of the impedance change from the same notch when this located far from the edge. As shown in Fig. 9, the edge notch has a much larger magnitude. A full parametric analysis for further studying this behavior is currently underway.

For an edge scan, the probe is moved parallel to the edge and therefore parallel with the $y$-axis (see Fig. 1). Edge scan measurements were carried out using the coil and notch characterized by the parameters given in Table III. While keeping its axis vertical, the coil is moved incrementally along a line parallel to the edge with the coil axis a distance 9.7 mm inbound from the edge, a value equal to its outer radius, and 11.7 mm from

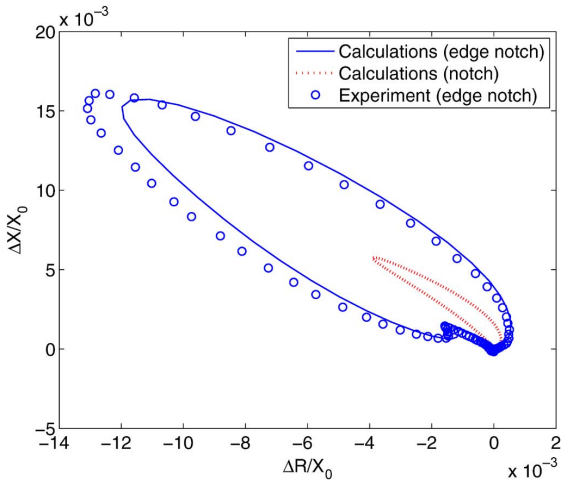


Fig. 9. Variation in normalized impedance of an induction coil with position due to a 4.98 mm long, 5.00 mm deep notch at the edge of an aluminum block; see Table II for test parameters. Results are the same as those used to plot the graphs shown in Fig. 8. Circles represent experimental data with the edge effect subtracted off and solid line shows theoretical predictions of notch signal.

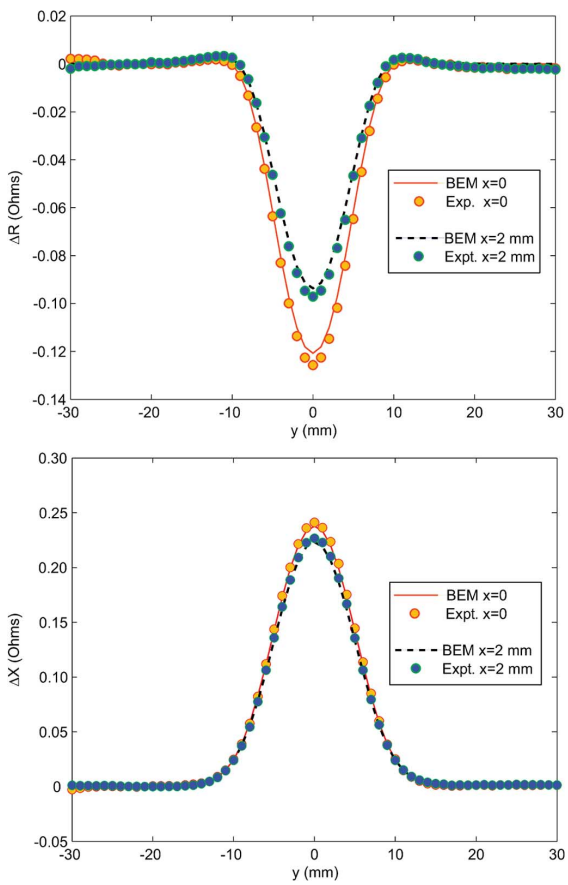


Fig. 10. Variation in normalized resistance and reactance of an induction coil with position due to a rectangular notch at the edge of an aluminum block. Coil is excited at 1 kHz and moved along the edge with its axis vertical, 9.7 and 11.7 mm inbound from the edge. Notch is in a plane $y = 0$ as illustrated in Fig. 1. Test parameters are given in Table III.

the edge, an extra 2 mm inbound. The coil impedance is determined as a function of position at 1 and 10 kHz as shown in Figs. 10 and 11, respectively. Clearly, there is good agreement between theory and experiment even though there are only 49 unknowns ($7 \times 7$) needed for the calculations of impedance at

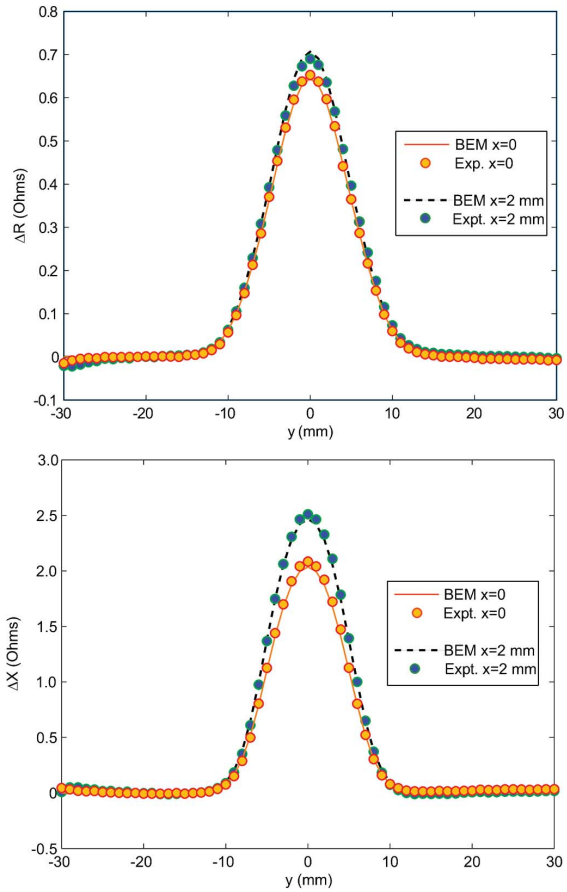


Fig. 11. Variation in normalized resistance and reactance of an induction coil with position due to a rectangular notch at the edge of an aluminum block. Coil, excited at 10 kHz, is moved along the edge with its axis vertical, either 9.7 and 11.7 mm inbound from the edge. Notch is in a plane $y = 0$ as illustrated in Fig. 1. Test parameters are given in Table III.

1 kHz and 147 ($7 \times 21$) for impedance calculations at 10 kHz. An impedance plane plot of the same data is shown in Fig. 12 together with results from impedance calculations using the finite element method (FEM).

## VIII. Conclusion

A model of the interaction of eddy currents with a crack at the corner of a quarter-space has been developed to compute fast and accurate predictions of probe signals due to edge cracks. Experimental results indicate that the predictions based on a volume element scheme are reasonably accurate. Because calculations that make use of a dedicated kernel need very few unknowns, the results can be computed extremely rapidly, typically in just a few seconds once the system matrix has been computed.

We computed predictions obtained with a dedicated kernel for a conductive quarter-space and demonstrated that the results are in good agreement with experiment. Similar calculation could also be performed for a crack at the edge of a hole or at the edge of a plate by adapting the truncated domain approach used for the present problem. The central task is to derive a suitable kernel in a convenient form for computing the matrix elements for the conductive region. The resulting kernel can then be used for either a boundary or volume element calculation of the flaw signal.

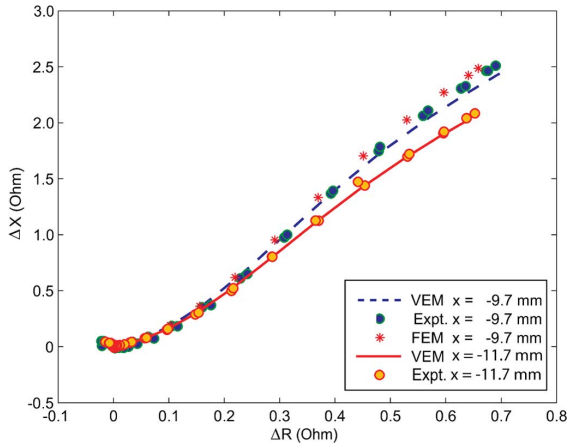


Fig. 12. Impedance plane plot of response of an induction coil interacting with a notch at the edge of an aluminum block. Coil, excited at 10 kHz, is moved along the edge with its axis vertical, 9.7 and 11.7 mm inbound from the edge. Notch is in a plane $y = 0$ as illustrated in Fig. 1. Test parameters are given in Table III. Experimental data is compared with both volume element and finite element calculations.

## APPENDIX
## MATRICES

The matrices introduced in (56), (57) and (58) are defined as follows. For the matrix in (56) we write

$$M[i,\ell] = M^{(1)}[i,\ell] + \alpha_\ell M^{(2)}[i,\ell] \tag{A1}$$

where

$$M^{(1)}[i,\ell] = \frac{2}{h_x}\int_0^c \sin u_i x \sin q_\ell x dz = \frac{1}{h_x}\begin{cases} \frac{\sin[c(q_\ell-u_i)]}{(q_\ell-u_i)} - \frac{\sin[c(q_\ell+u_i)]}{(q_\ell+u_i)} & q_\ell \neq u_i \\ c - \frac{\sin 2cu_i}{2u_i} & q_\ell = u_i \end{cases} \tag{A2}$$

and

$$M^{(2)}[i,\ell] = \frac{2}{h_x}\int_c^h \sin u_i x \cos p_\ell (h_x - x) dx = \frac{1}{h_x}\begin{cases} \frac{\cosh_x u_i - \cos[(h_x-c)p_\ell + cu_i]}{p_\ell - u_i} \\ -\frac{\cos h_x u_i - \cos[(h_x-c)p_\ell - cu_i)]}{p_\ell+u_i} & p_\ell \neq u_i \\ (h_x - c)\sin h_x u_i \\ +\frac{1}{2u_i}[\cos(h-2c)u_i - \cos h_x u_i] & p_\ell = u_i \end{cases} \tag{A3}$$

We also write

$$M_a[i,\ell] = M_a^{(1)}[i,\ell] + \alpha_\ell \frac{p_\ell}{q_\ell} M_a^{(2)}[i,\ell] \tag{A4}$$

where

$$M_a^{(1)}[i,\ell] = \frac{2}{h_x}\int_0^c \cos u_i x \cos q_\ell x dx = \frac{1}{h_x}\begin{cases} \frac{\sin[c(q_\ell-u_i)]}{(q_\ell-u_i)} + \frac{\sin[c(q_\ell+u_i)]}{(q_\ell+u_i)} & q_\ell \neq u_i \\ c + \frac{\sin 2cu_i}{2u_i} & q_\ell = u_i \end{cases} \tag{A5}$$

and

$$M_a^{(2)}[i,\ell] = \frac{2}{h_x}\int_c^h \cos u_i x \sin p_\ell (h_x - x) dx = \frac{1}{h_x}\begin{cases} \frac{\cos h_x u_i - \cos[(h_x-c)p_\ell + cu_i]}{p_\ell - u_i} \\ +\frac{\cos h_x u_i - \cos[(h_x-c)p_\ell - cu_i)]}{p_\ell+u_i} & p_\ell \neq u_i \\ (h_x - c)\sin h_x u_i \\ -\frac{1}{2u_i}[\cos(h-2c)u_i - \cos h_x u_i] & p_\ell = u_i \end{cases} \tag{A6}$$

Finally, we define

$$M_b[i,\ell] = \frac{2}{h_x}\int_0^c \cos u_i x \cos r_\ell x dx = \frac{1}{h_x}\begin{cases} \frac{\sin[c(r_\ell-u_i)]}{(r_\ell-u_i)} + \frac{\sin[c(r_\ell+u_i)]}{(r_\ell+u_i)} & r_\ell \neq u_i \\ c + \frac{\sin 2cu_i}{2u_i} & r_\ell = u_i \end{cases} \tag{A7}$$

## REFERENCES


[1] D. McKirdy, "Recent improvements to the application of the volume integral method of eddy current modeling," *J. Nondestr. Eval.*, vol. 8, no. 1, pp. 45–52, 1989.

[2] J. R. Bowler, S. A. Jenkins, L. D. Sabbagh, and H. A. Sabbagh, "Eddy-current probe impedance due to a volumetric flaw," *J. Appl. Phys.*, vol. 70, no. 3, pp. 1107–1114, 1991.

[3] J. R. Bowler, "Eddy-current interaction with an ideal crack. I. The forward problem," *J. Appl. Phys.*, vol. 75, no. 12, pp. 8128–8137, 1994.

[4] T. Theodoulidis, N. Poulakis, and A. Dragogias, "Rapid computation of eddy current signals from narrow cracks," *NDT&E Int.*, vol. 42, pp. 13–19, 2010.

[5] Y. Yoshida and J. R. Bowler, "Vector potential integral formulation for eddy-current response to cracks," *IEEE Trans. Magn.*, vol. 36, no. 2, pp. 461–469, Apr. 2000.

[6] V. Monebhurrun, D. Lesselier, and B. Duchene, "Evaluation of a 3-D bounded defect in the wall of a metal tube at eddy current frequencies: The direct problem," *J. Electromagnetic Waves Applic.*, vol. 12, no. 2, pp. 315–347, 1998.

[7] J. R. Bowler and T. P. Theodoulidis, "Boundary element calculation of eddy currents in cylindrical structures containing cracks," *IEEE Trans. Magn.*, vol. 45, no. 3, pp. 1012–1015, Mar. 2009.

[8] W. C. Chew, *Waves and Fields in Inhomogeneous Media*. New York: IEEE Press, 1995.

[9] T. P. Theodoulidis and J. R. Bowler, "Eddy current coil interaction with a right-angled conductive wedge," *Proc. Roy. Soc. Lond. A*, vol. 461, no. 2062, pp. 3123–3139, 2005.

[10] T. P. Theodoulidis and J. R. Bowler, "Interaction of an eddy-current coil with a right-angled conductive wedge," *IEEE Trans. Magn.*, vol. 46, no. 4, pp. 1034–1042, Apr. 2010.

[11] J. R. Bowler and T. P. Theodoulidis, "Coil impedance variation due to induced current at the edge of a conductive plate," *J. Phys. D: Appl. Phys.*, vol. 39, no. 13, pp. 2862–2868, 2006.

[12] J. R. Bowler, T. P. Theodoulidis, H. Xie, and Y. Ji, "Evaluation of eddy current probe signals due to cracks in fastener holes," *IEEE Trans. Magn.*, vol. 48, no. 3, pp. 1159–1170, Mar. 2012.

[13] L. B. Felsen and N. Marcuvitz, *Radiation and Scattering of Waves.*. Englewood Cliffs, NJ: Prentice-Hall, 1973.

[14] L. M. Delves and J. N. Lyness, "A numerical method for locating the zeros of an analytical function," *Math. Comp.*, vol. 21, no. 100, pp. 543–560, 1967.

[15] J. N. Lyness, "Numerical algorithms based on the theory of complex variable," in *Proc. ACM*, 1967, pp. 125–133.

[16] M. Dellnitz, O. Schutze, and Q. Zheng, "Locating all the zeros of an analytic function in one complex variable," *J. Comp. Math.*, vol. 138, pp. 325–333, 2002.